Structural, Electrical and Electrochemical Properties of Fe Doped Orthosilicate Cathode Materials

Nirbhay Singh, Komal Kanwar, Shweta Tanwar, A. L. Sharma, and B. C. Yadav

Abstract We report the paper related to the effect of Fe doping on the $Li_2Fe_xMn_{1-x}SiO_4$ ($x = 0, 0.1, 0.2, 0.3, 0.4, 0.5$) cathode materials synthesized by Sol-Gel technique. X-Ray Diffraction evidences the monoclinic structure with space group *Pn(7)* and crystal size decreases from 43 to 35 nm on doping Fe in Li_2MnSiO_4. Field emission scanning electron microscopy (FESEM) confirms that particle size reduces from 60 to 21 nm with increase of Fe concentration. The impedance analysis shows that highest electrical conductivity was 4.5×10^{-5} Scm^{-1} for $Li_2Fe_{0.4}Mn_{0.6}SiO_4$ cathode material. The initial specific capacity was 152 $mAhg^{-1}$ at the rate of 0.1 C and 131 $mAhg^{-1}$ after the 50th cycle with 86% capacity retention. The doping of Fe enhanced the conductivity by reducing its charge transfer resistance and increasing Li-ion diffusion coefficient than the pure Li_2MnSiO_4 cathode material.

Keywords Orthosilicate · Cathode material · Electrochemical properties · Lithium-ion batteries

1 Introduction

The energy plays a key role in economic development of any nation so each country is trying to set itself as an independent centre in production and storage of energy [1]. Today, the major part of electricity is produced with the help of non-renewable resources which come to ends till 40–70 years, so it is a big challenge in front of the world to generate electricity by using some renewable sources of energy which would be cost effective and easily available [2]. The most popular renewable energy

N. Singh · B. C. Yadav
Department of Physics, BabaSaheb Bhimrao Ambedakar University, Lucknow, UP, India

N. Singh · K. Kanwar · S. Tanwar · A. L. Sharma (✉)
Department of Physics, Central University of Punjab, Bathinda, Punjab, India
e-mail: alsharma@cup.edu.in

K. Kanwar
Department of Physics, Central University of Rajasthan, Ajmer, Rajasthan, India

S. B. Krupanidhi et al. (eds.), *Advanced Functional Materials and Devices*, Springer Proceedings in Materials 14, https://doi.org/10.1007/978-981-16-5971-3_26

resources in order to replace conventional resources produced from hydrocarbon are: solar cells, fuel cells and supercapacitors and Lithium-ion batteries [3]. The Li_2MnSiO_4, shows a higher theoretical capacity of 334 $mAhg^{-1}$ which is obtained on the basis of two redox couples of Mn^{2+}/Mn^{3+} and Mn^{3+}/Mn^{4+} and also provides a higher cell potential at ~4.0 V, than Li_2FeSiO_4 which have a theoretical capacity 166 $mAhg^{-1}$ and cell potential ~3.0 V. On the basis of exhaustive literature reports, it is confirmed that the practical capacity limitation can be improved via doping of Fe in place of Mn cation with different wt% to optimize the concentration.

In the present study, we prepared $Li_2Fe_xMn_{1-x}SiO_4$ cathode material by sol-gel method with different concentrations of Fe doping at 900 °C for 12 h. The effect of Fe doping on the crystal structure, morphology, electrical properties and Li^+ diffusion coefficient was discussed. To improve the poor electronic conductivity of Li_2MnSiO_4 which is ~10^{-15} Scm^{-1} at room temperature [4], we doped Fe in the ratio $x = 0, 0.1, 0.2, 0.3, 0.4$ and 0.5 and investigated the effect of Fe doping on Li_2MnSiO_4 on their electrochemical properties.

2 Experimental

2.1 Precursor Solution

The precursor solution was prepared by dissolving an appropriate amount of $LiNO_3$, $MnCo_3$, $Fe(NO_3)_3$ and SiO_2 in distilled water. To hydrolyze the dissolved solution some droplets of citric acid were added to the precursor solution.

2.2 Preparation of $Li_2Fe_xMn_{1-x}SiO_4$

$Li_2Fe_xMn_{1-x}SiO_4$ was prepared by **sol-gel** synthesis method. The prepared cathode material is label as LFMS and it is prepared for varying the concentration of Fe for $x = 0.1, 0.2, 0.3, 0.4, 0.5$ so label as LFMS-1, LFMS-2, LFMS-3, LFMS-4, LFMS-5 respectively (Fig. 1).

2.3 Characterization Technique

The crystal structure of $Li_2Fe_xMn_{1-x}SiO_4$ was identified by X-Ray powder diffraction (model: Philips. Field emission scanning electron microscopy (FESEM; Merlin Compact). Fourier Transform Infra-red (FTIR) Spectroscopy (Model: Tensor 27. Electrical properties measurements are carried out by CH instrument (Model: 760) from which Electrical Impedance Spectroscopy (EIS) is used to calculate the electrical conductivity of prepared material, Cyclic Voltammetry (CV) is used to find out the power capacity of the prepared materials.

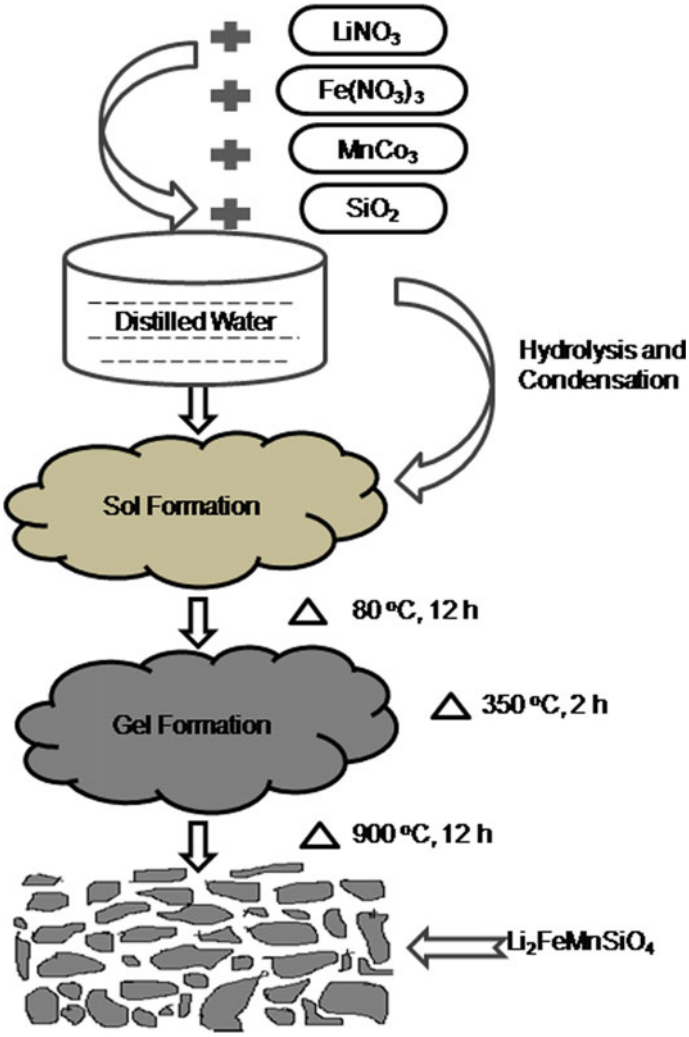

Fig. 1 Schematic diagram of Sol-gel method

3 Results and Discussion

1. **X-Ray Powder Diffraction Analysis (XRD)**
   The X-ray powder diffraction (XRD) of dilithium silicate materials comprising of $Li_2Fe_xMn_{1-x}SiO_4$ ($x = 0$, 0.1, 0.2, 0.3, 0.4 and 0.5) synthesized by sol-gel method at 900 °C are given in Fig. 2. The diffraction analysis has been performed in the wide angle $2\theta = 10°$ to 80^0. The diffraction peaks at 27°, 33°, 38°, 42°, 55° and 65° are associated with the planes (012), (131), (112), (240), (161) and (023) respectively. All the obtained peak intensity closely matches with JCPDS [file

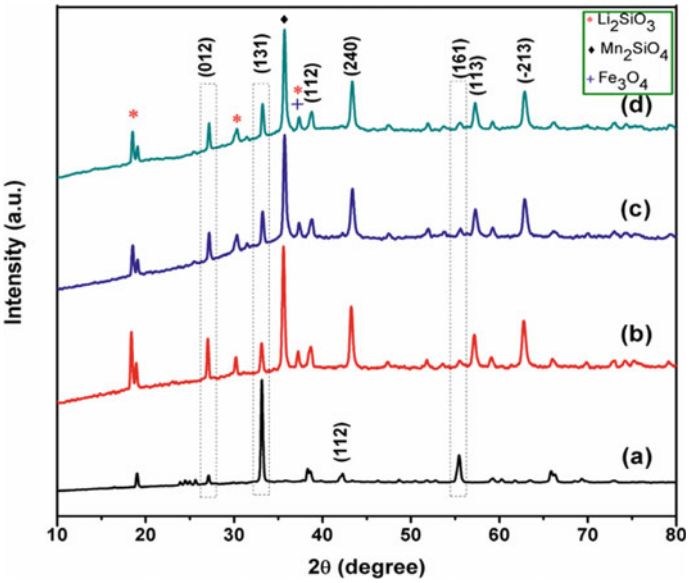

Fig. 2 X-ray diffraction pattern of $Li_2Fe_xMn_{1-x}SiO_4$ **a** $x = 0$, **b** $x = 0.3$, **c** $x = 0.4$ and **d** $x = 0.5$

no. 00-055-0704] file which confirms the monoclinic structure of the samples with space group *Pn(7)*. The impurity phases like Li_2SiO_3 was also presents at an angle 19°, 30°, 37° and Mn_2SiO_4 at angle 35° [5] and Fe_3O_4 at angle 37° in $Li_2Fe_xMn_{1-x}SiO_4$ which are unavoidable. The sifting in peaks occurs firstly at a higher angle (from $x = 0$ to 0.4) after that it starts sifted towards a lower angle (from $x = 0.4$ to 0.5). The shifting in peaks directly correlate with the particle size which shows firstly the crystal size decrease as dopant concentration increases from $x = 0$ to 0.4. The lowest value of size for the $x = 0.4$ will enhance its electrochemical properties like electrical conductivity, energy density, cycle life, etc. which will be analyzed later. The intensity of peaks also first increase from $x = 0$ to 0.4 and after that decreases from $x = 0.4$ to 0.5. All the major peaks of pure Li_2MnSiO_4 are also present after the Fe doping, so there is no strong evidence is observed for structure changes after doping of Fe in pure Li_2MnSiO_4 material.

2. **Field Emission Scanning Electron Microscopy (FESEM) Analysis**

The morphological study was studied by using FESEM. The Fig. 3a shows the surface morphology of pure Li_2MnSiO_4 cathode material. There is no agglomeration between the particles and the calculated average size is about 47 nm. Figure 3b-f shows the surface morphology of $Li_2Mn_xFe_{1-x}SiO_4$ cathode material ($x = 0.1, 0.2, 0.3, 0.4$ and 0.5). As the concentration of Fe increases, particle size reduces because of this the lithium-ion path length decreases and this results in improvement in electrochemical Properties [6]. The possible reason for the reduction in particle size is the decrease in internal stress may increase its binding

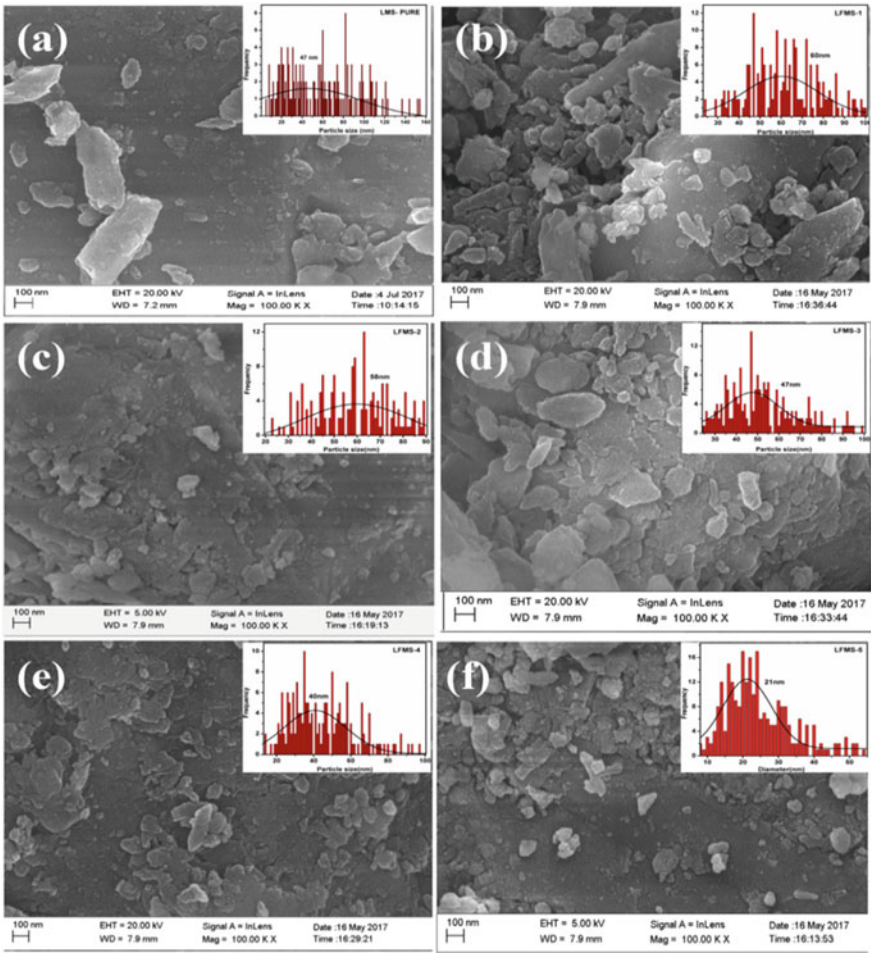

Fig. 3 FESEM images of $Li_2Fe_xMn_{1-x}SiO_4$ **a** $x = 0$, **b** $x = 0.1$, **c** $x = 0.2$ and **d** $x = 0.3$, **e** $x = 0.4$, **f** $x = 0.5$

force with a relative area of its grain boundaries. Particle size calculated from the FESEM is 47, 60, 58, 47, 40 and 20 (all in cm) for LMS, LFMS-1, LFMS-2, LFMS-3, LFMS-4 and LFMS-5 respectively.

3. **Fourier Transform Infra-red Radiation (FTIR)**
FTIR is a powerful technique to identify the functional group, impurity and their bonding with the host material present in the material. FTIR was done in the wavenumber range 400–4000 cm^{-1} with the transmission mode for $Li_2Fe_xMn_{1-x}SiO_4$ material which is given in Fig. 4. The transmission peaks are obtained at 525, 550, 619, 737, 852, 951 and 1070 cm^{-1}. The presence of tetrahedral SiO_4 group was confirmed by FTIR. The vibrational peaks observed

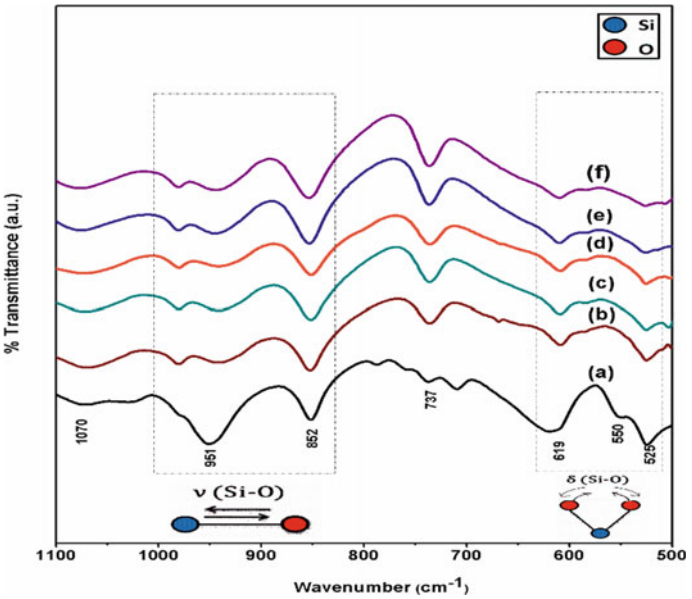

Fig. 4 FTIR spectra of $Li_2Fe_xMn_{1-x}SiO_4$ **a** $x = 0$, **b** $x = 0.1$, **c** $x = 0.2$ and **d** $x = 0.3$, **e** $X = 0.4$, **f** $x = 0.5$

at 951 and 852 cm^{-1} are associated with the stretching vibration of O–Si–O bonds in tetrahedral SiO_4 group. The minor peak at 737 cm^{-1} in Fig. 4 is attributed to bending vibrations of Si–O–Si bonds. There is also an increase or decrease in peak intensity which occurs due to an increase or decrease in the amount of material present in the material. Here, the intensity of peak at 737 cm^{-1} is increases with an increase in the Fe dopant concentration. The vibrational bands at 525, 550 and 619 cm^{-1} is corresponds to bending vibrations of O–Si–O bonds in tetrahedral SiO_4 group [7]. There is a decrease in the peak intensity. The vibrational bands at 1070 cm^{-1} can correspond to Si–O vibrations in Li_2SiO_3. The shifting in peaks also occurs at higher wavenumber as the dopant concentration increases.

Electrochemical Analysis

These analyses are done with an electrochemical workstation CH-760 instrument. The main technique performed are EIS (Electrochemical Impedance Spectroscopy), CV (Cyclic Voltammetry) and GCD (Galvonostatic charge and discharge).

4. **Impedance Spectroscopy Study**

The impedance spectroscopy (Nyquist plot) is performed between the real part and imaginary part of impedance. The prepared cathode materials were sandwiched between two blocking (stainless steel) electrodes and small ac voltage (10 mV) applied in frequency range of 1 Hz to 1 MHz. Figure 5

shows the impedance spectroscopy results of $Li_2Fe_xMn_{1-x}SiO_4$ materials [8]. In order to validate the experimentally obtained data, a nonlinear least square fitting means of ZSImpWin software is performed. On fitting, it is observed that all the experimental data fitted with a series combination of constant phase elements with resistance followed by parallel combination of another constant phase element. Constant phase element (CPE) may be considered as the practical representation of capacitance. In general, it is intermingling of both (resistance and capacitance). The constant phase element can be represented by the formulae:

$$\text{CPE} = \frac{1}{(\omega Q_o)^n}$$

where ω is angular frequency and 'n' is power exponent. The value of $n = 1$ represent the CPE is pure capacitance, $n = 0$ pure resistance and $n = -1$ represents pure inductance. If the n value lies in between 0 and 1 that represents the presence of resistance and capacitance both. The estimated value of bulk resistance from the experiment as well as through fitting was obtained in the range of 6–12 kΩ.

5. **Electrical Conductivity Analysis**

The electrical conductivity of all prepared cathode material samples is obtained using the above discussed impedance spectroscopy results. As the bulk resistance obtained by the line joining of intercept of lower frequency spike and high frequency small semi-circular arc. The formula for estimation of bulk electrical conductivity (σ_{dc}) from bulk resistance is given below:

$$\sigma_{dc} = \frac{1}{R_b}\frac{\ell}{A}$$

where ℓ is sample thickness, A is contact area of electrode and R_b is the bulk resistance of the material calculated from Nyquist plot [9].

From Fig. 5a–f, the estimated value of bulk resistance of LMS, LFMS-1, LFMS-2, LFMS-3, LFMS-4 and LFMS-5 are 6931, 6043, 4708, 3674, 416 and 12,063 Ω respectively with the thickness value $t = 0.02$ cm and $A = 1.07$ (cm^2) for each sample. Conductivity calculated from the bulk resistance is of the order of 2.7×10^{-6}, 3.1×10^{-6}, 4.0×10^{-6}, 5.1×10^{-6}, 4.5×10^{-5} and 1.6×10^{-6} S cm^{-1} for LMS, LFMS-1, LFMS-2, LFMS-3, LFMS-4 and LFMS-5 respectively. As the concentration of dopant-Fe increases, value of electrical conductivity increases this may be possible. The conductivity of the doped sample material is one order higher than the pure material recorded.

6. **Cyclic Voltammetry Analysis**

Cyclic voltammetry (CV) is generally performed in between the definite electrochemical potential through charging and discharging of complete

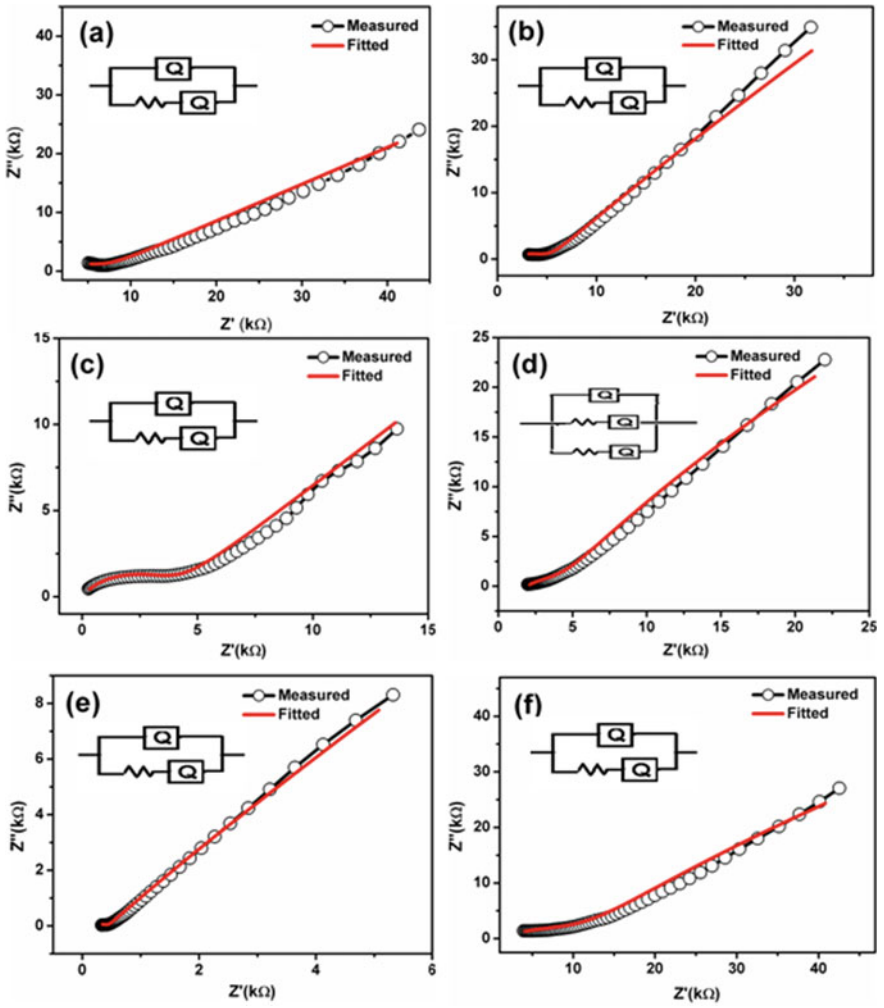

Fig. 5 Impedance spectra of $Li_2Fe_xMn_{1-x}SiO_4$ **a** $x = 0$, **b** $x = 0.1$, **c** $x = 0.2$ and **d** $x = 0.3$, **e** $x = 0.4$, **f** $x = 0.5$

system. It is performed on different scan rates depend upon the current (sensitivity) limit. CV measurement is done between current (Y axis) and potential (X axis) on certain scan rate. The area under the curve directly useful in estimating the energy of the system. The energy density of the system can also be estimated in unit volume or mass based on necessity. During this charging and discharging oxidation and reduction takes place at the anode and cathode invariably. The liberation and deintercalation of lithium ions taken place due to the use of variable oxidation state transition metal ions. This redox reaction use to determine using this technique [10].

Figure 6 shows the cyclic voltammogram of di lithium manganese silicate (Li_2MnSiO_4) and Fe doped di lithium manganese silicate with different weight percent concentrations. Cyclic voltammetry graphs are studied at different scan rates (~0.1 mV/s) for different prepared materials shown in Fig. 6. The power capacity is calculated by multiplying the area of CV curve and current which is 96, 106, 263, 311, 357 and 239 for x = 0, 0.1, 0.2, 0.3, 0.4 and 0.5 respectively. The power capacity is larger for $Li_2Fe_{0.4}Mn_{0.6}SiO_4$ cathode material than the pure sample which indicates that this material is having highest capacity for lithium intercalation or deintercalation process.

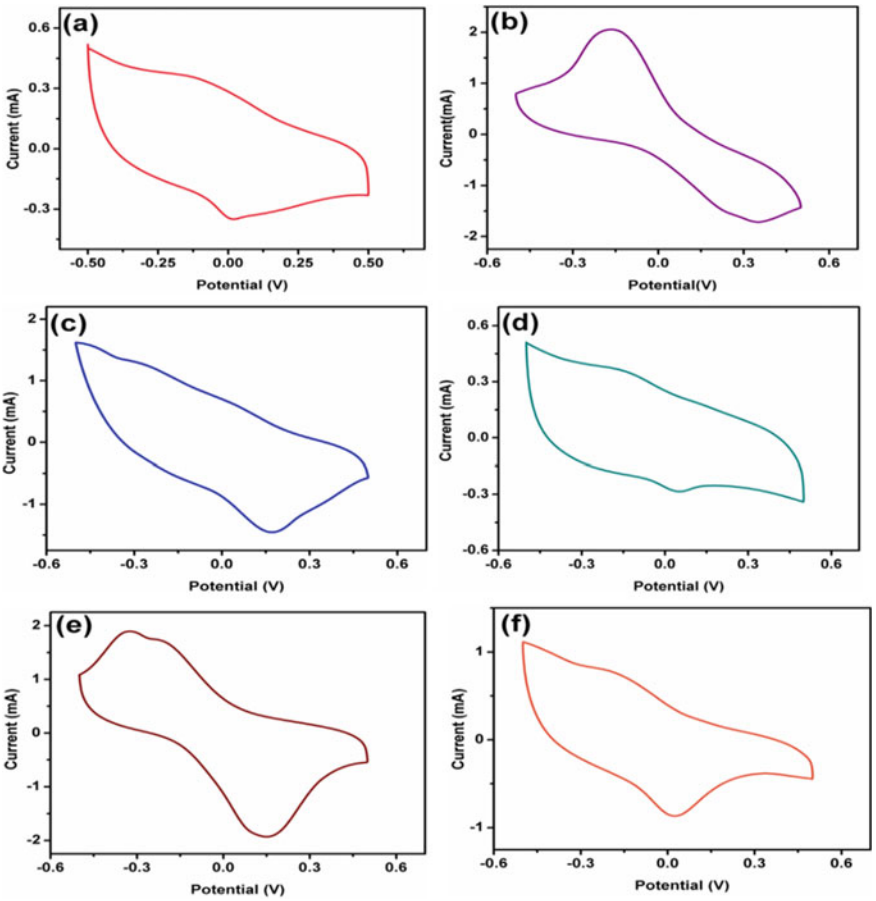

Fig. 6 Cyclic—voltammetry graphs of $Li_2Fe_xMn_{1-x}SiO_4$ **a** $x = 0$, **b** $x = 0.1$, **c** $x = 0.2$ and **d** $x = 0.3$, **e** $x = 0.4$, **f** $x = 0.5$

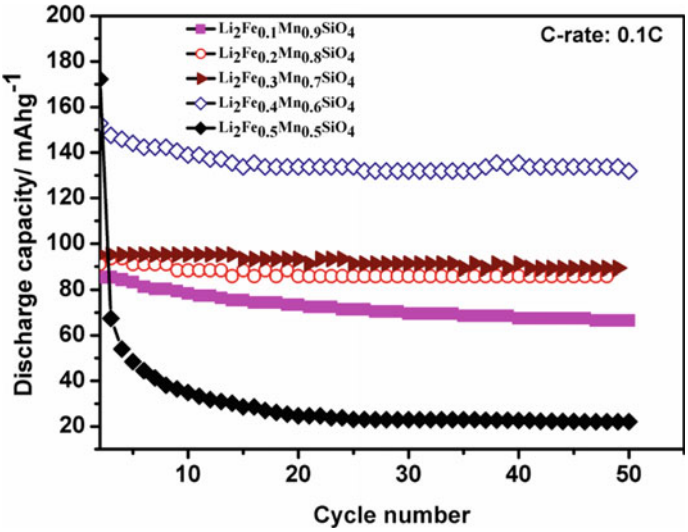

Fig. 7 Retention capacity graphs of $Li_2Fe_xMn_{1-x}SiO_4$ **a** $x = 0.1$, **b** $x = 0.2$, **c** $x = 0.3$ and d $x = 0.4$, **e** $x = 0.5$

Capacity Retention Analysis

This study provides the capacity retention behaviour in Charging and discharge cycle. Here it is observed on increasing the Fe concentration the value of Discharge capacity increases which is in correlation with electrochemical analysis other studies like CV.

The $Li_2Fe_{0.4}Mn_{0.6}SiO_4$ cathode material gives remarkable results with a discharge capacity 152 mAh/g initially and it is stable after 50 cycles up to 131 mAh/g value of discharge capacity. This material is meeting our expectations. So this material shows good cyclic stability behaviour. For the cathode material Li_2MnSiO_4 if we enhance its all properties then we have to dope Fe at the concentration of 0.4.

The discharge capacity for $Li_2Mn_xFe_{1-x}SiO_4$ is 85, 93, 95, 152, 172 and after 50 cycle it is 66, 85, 89, 131, for $x = 1$, 0.1, 0.2, 0.3, 0.4 and 0.5 respectively (Fig. 7).

References

1. Joshua KP, Mohanalin J, Christa SJ, Bhuvanesh A (2021) A novel autonomous energy management system: solution for a fossil fuel free future. In: Advances in automation, signal processing, instrumentation, and control: select proceedings of i-CASIC 2020, 163
2. Wu W, Sun Z, He Q, Shi X, Ge X, Cheng J, Zhang Z (2021) Boosting lithium-ion transport kinetics by increasing the local lithium-ion concentration gradient in composite anodes of lithium-ion batteries. ACS Appl Mater Interfaces
3. Jacome A, Dépature C, Boulon L, Solano J (2021) A benchmark of different starting modes of a passive fuel cell/ultracapacitor hybrid source for an electric vehicle application. J Energy Storage 35:102280

4. Liu P, Gong Y, Nie S, Fu Q, Li L, Liu N, Chen J (2019) The porous spherical Mn and Ti co-doped Li_2FeSiO_4/C cathodes material for lithium-ion batteries. Ionics 25(8):3611–3621
5. Hergett W, Neef C, Meyer HP, Klingeler R (2021) Challenges in the crystal growth of Li_2FeSiO_4. J Cryst Growth 556:125995
6. Qiu H, Jin D, Wang C, Chen G, Wang L, Yue H, Zhang D (2020) Design of Li_2FeSiO_4 cathode material for enhanced lithium-ion storage performance. Chem Eng J 379:122329
7. Hsu CH, Du TR, Tsao CH, Lin HP, Kuo PL (2019) Hollow Li_2FeSiO_4 spheres as cathode and anode material for lithium-ion battery. J Alloy Compd 797:1007–1012
8. Duan WY, Li T, Li SD, Gao K (2019) Energy storage mechanism of powdery and nano-fibrous Li2FeSiO4 as aqueous capacitor electrode. Mater Lett 250:79–83
9. Thayumanasundaram S, Rangasamy VS, Seo JW, Locquet JP (2019) Novel strategies to improve the structural and electrochemical stability of Li_2CoSiO_4 during cycling. Solid State Ionics 337:161–169
10. Yang F, Xia Z, Huang S, Zhang X, Song Y, Xiao G, Shao G, Liu Y, Deng H, Jiang D, Ouyang Z (2020) High field phase transition of cathode material Li2MnSiO4 for lithium-ion battery. Mater Res Expr 7(2):026104